Ab initio study of EMIM-BF_4 molecule adsorption on Li surfaces as a model for ionic liquid/Li interfaces in Li-ion batteries

Hubert Valencia,* Masanori Kohyama, Shingo Tanaka, and Hajime Matsumoto
Research Institute for Ubiquitous Energy Devices, National Institute of Advanced Industrial Science and Technology, 1-8-31, Midorigaoka, Ikeda, Osaka 563-8577, Japan
(Received 12 August 2008; published 3 November 2008)

The adsorption of 1-ethyl-3-methyl imidazolium tetrafluoroborate (EMIM-BF_4) molecules onto Li (100), (110), and (111) surfaces is investigated by means of periodic density-functional theory calculations as a model for room-temperature ionic liquid/Li-metal anode interfaces in a Li-ion battery. We examined the atomic and electronic structures of isolated $EMIM^+$ and BF_4^- molecules, a pair of $[EMIM]^+[BF_4]^-$, and Li bulk and surfaces, which are in good agreement with previous theoretical and experimental results. We observed that the EMIM-BF_4 adsorption generally induces significant changes on the Li surfaces. One or two Li-surface atoms are greatly attracted to the BF_4 anion, resulting in electronic density depletion at the attracted Li atoms while the electrons are attracted toward the EMIM cation, regardless of the coordination mode of adsorption or the kinds of Li surfaces. These features represent the tendency of easy ionization of Li and Li_x-BF_4-cluster formation, coupled with reduction in $EMIM^+$, which is in contrast to the EMIM-BF_4 adsorption on a Au (100) surface without any displacements of Au atoms or any specific electronic behavior to reduce $EMIM^+$.

DOI: 10.1103/PhysRevB.78.205402 PACS number(s): 68.43.Bc, 73.20.−r, 82.65.+r

I. INTRODUCTION

Since the late 1990s, room-temperature ionic liquids (RTILs) have become the focus of an always growing interest due to their remarkable properties such as a low vapor pressure, a low melting point, nonflammability, and high ionic conductivity.[1] These properties make RTILs candidates for numerous applications. More precisely, RTILs are expected as electrolytes in rechargeable Li-ion batteries,[2,3] which are indispensable energy storage devices for use in portable electronic equipments and electric vehicles. In such systems, the safety owing to the nonflammability of RTILs is not the only advantage but the RTIL electrolyte enables us to use pure Li-metal anode electrode for the batteries with higher energy density,[4–7] whereas traditional systems rely on graphite or alloy anodes,[8] due to the serious dendrite formation problem of Li-metal electrode.[9] The dendrite formation can be prevented by the RTIL electrolyte although the clear reason has not yet been found.

There exist no theoretical studies on RTIL/electrode systems with respect to electrochemistry. In fact, the interesting properties of these systems turn their representation by means of quantum chemistry or electronic theories to be a real challenge. Recent first-principles studies of RTILs[10–21] focus on the analysis of the nature of atomic bonding, static or dynamical structural features, and ionic transport properties but little is known about their interactions with cathode or anode electrodes. Investigation of such interactions, especially RTIL/Li-metal anode interactions, is a key feature for a better understanding of Li-ion batteries using the RTIL electrolyte.

In this paper, as the first step, we examine the primary behavior of a pair of cation and anion molecules of a typical RTIL, 1-ethyl-3-methyl imidazolium tetrafluoroborate (EMIM-BF_4),[22,23] adsorbed on several kinds of low index Li surfaces by using periodic density-functional theory (DFT) calculations. Of course, for a better description of the electrochemical system, the charged electrode should be considered together with the resulting electrostatic field. Even if such calculations are now accessible, within for example the scheme proposed by Otani and co-workers,[24,25] the present study focuses on the analysis of the primary interactions between RTIL molecules and Li-metal surfaces without any external charges.

Generally, constituent molecules of RTILs have specific ionic charges generating long-range electrostatic fields, and thus the interactions with metal surfaces should have quite different features from usual molecular adsorption on metal surfaces, which should have some similarity to metal/ionic solid interfaces.[26–28] On the other hand, Li is known as the metal with the highest ionization tendency. Thus we also examine the EMIM-BF_4 adsorption on a Au surface for comparison in order to clarify the general and special features of EMIM-BF_4/Li systems.

In this paper, the theoretical scheme is explained in Sec. II. In Secs. III A and III B, Li bulk and surfaces, isolated $EMIM^+$ and BF_4^- molecules, and a pair of $[EMIM]^+[BF_4]^-$ are examined by the present scheme as compared with previous theoretical and experimental results. Examination of RTIL molecules is quite important because of rare computations by the present type of schemes compared with molecular-orbital calculations. In Sec. III C, we examine the EMIM-BF_4 adsorption on Li and Au surfaces. In Sec. III D, we discuss the nature of interfacial charge transfer, and we give concluding remarks in Sec. IV.

II. METHODOLOGY

Chemical systems are represented by three-dimensional (3D)-periodic supercells, and the electronic and structural properties are determined by the DFT using the Vienna *Ab initio* Simulation Package (VASP) software.[29,30] The exchange-correlation functional chosen was that of Perdew and Wang (PW91) (Ref. 31) within the generalized gradient

approximation (GGA). Valence electrons are dealt with in the framework of the projector augmented wave (PAW) scheme.[32,33] This methodology is referred to as PAW-PW91-GGA. For comparison, Perdew, Brucke, and Ernzerhof functional[34] was also examined for Li-metal systems, which are referred to as PAW-PBE96-GGA. A cut-off energy for the plane-wave basis is 550 eV chosen to be sufficient for every system optimization. The *k*-point sampling for metallic systems is performed by a Monkhorst and Pack scheme[35,36] while only gamma point is used for isolated molecular systems, treating the band dispersion effects as being unnecessary. An isolated charged molecule is dealt with in a large box by subtracting or adding one electron with a homogeneous background countercharge assumed. Monopole, dipole, and quadrupole interactions with periodic images are removed as described in Refs. 37 and 38, within a more general approach. The structural optimization is performed with a criterion of 10^{-4} eV for energy and 10^{-3} eV/Å for atomic forces. This methodology usually gives results with the accuracy of (i) 5 meV in energy and (ii) 0.01 Å in distance.

The atomic charges are analyzed using a Voronoi decomposition[39–41] of the total charge density, where space is divided for each atomic polyhedral. This mathematical decomposition is often used in several science areas while its drawback is not taking into account the difference between species. However, it often leads to a good result in dealing with charge changes between some fragments. The local density of states (LDOS) is obtained by the projection to each Wigner-Seits sphere with the radius of the PAW projectors. The spin-polarization computations are only performed for EMIM and BF_4 radicals with odd numbers of valence electrons.

III. RESULTS AND DISCUSSION

A. Lithium

Although a body-centered-cubic (bcc) lattice is not the equilibrium 0 K form of Li crystal,[42] we take this geometry because of the usual experimental observation of bcc Li at room temperature. The bulk bcc structure was optimized using the present scheme. Note that 1*s* electrons of Li are dealt with as valence electrons owing to the semicore nature. The cohesive energy is defined against the reference atomic energy of Li, obtained by a calculation of a single Li atom in a large $13\times13\times13$ Å^3 cubic box. The lattice parameter (3.450 Å) and cohesive energy (1.619 eV) by PAW-PW91-GGA are consistent with previous experimental (3.48 Å and 1.66 eV in Ref. 43) and theoretical works (3.46 Å and 1.61 eV in Ref. 44, and see Table III in Ref. 44). The difference in the cohesive energy between PW91 and PBE96 is within tenth of an electron volt, and the lattice parameter changes from 3.4496 (PW91) to 3.4449 Å (PBE96).

For the surface calculations, we constructed the (100), (110), and (111) surface slabs using the optimized bcc lattice parameter. For each (1×1) surface cell, we examined several numbers of atomic layers with enough vacuum regions ($\sim$10 Å). For the relaxation of the surface slab, only one surface is relaxed with the bottom two layers of the slab fixed. Thus the surface energy is defined as

$$\sigma = \underbrace{\frac{1}{A}(E_{\text{opt}}^{\text{slab}} - NE^{\text{bulk}})}_{\text{opt and bcc positioned}} - \underbrace{\frac{1}{2A}(E_{\text{init}} - NE^{\text{bulk}})}_{\text{one bcc positioned}}, \quad (1)$$

where A is the surface area, N is the number of Li atoms in the cell, E^{bulk} is the total energy per atom for bulk bcc Li, E_{init} is the total energy of the slab without relaxation, and $E_{\text{opt}}^{\text{slab}}$ is the total energy of the slab with one-side relaxation. Another way of getting the surface energy is to use slabs with different numbers of layers as mentioned in Eq. (1) of Doll *et al.*'s[44] paper for the case of a slab with both-side relaxation:

$$\sigma = \frac{1}{2A}\left\{E_{\text{opt}}^{\text{slab}}(n) - [E_{\text{opt}}^{\text{slab}}(n) - E_{\text{opt}}^{\text{slab}}(n-m)]\frac{n}{m}\right\}, \quad (2)$$

where $E_{\text{opt}}^{\text{slab}}(n)$ is the total energy of the n-layer slab with both-side relaxation, and the term $[E_{\text{opt}}^{\text{slab}}(n)-E_{\text{opt}}^{\text{slab}}(n-m)]\frac{n}{m}$ corresponds to the total energy of the bulk crystal consisting of n layers via computations with the same periodicity as the surface-slab cell. In a similar methodology for the surface slab with one-side relaxation, the surface energy is given as

$$\sigma = \frac{1}{A}[E_{\text{opt}}^{\text{slab}}(n) - E^{\text{bulk}}(n)] - \frac{1}{2A}[E_{\text{init}}(n) - E^{\text{bulk}}(n)], \quad (3)$$

where $E^{\text{bulk}}(n)=[E_{\text{init}}(n)-E_{\text{init}}(n-m)]\frac{n}{m}$ and $E_{\text{init}}(n)$ is the total energy of the n-layer surface slab without relaxation. $E^{\text{bulk}}(n)$ corresponds to the total energy of the bulk crystal consisting of n layers obtained by similar conditions as the surface-slab cell.

The calculated surface energies of Li by Eqs. (1) and (3) are listed in Table I. Results are consistent with other theoretical works[44,45] and the surface energies share almost the same energetic probabilities. There are no significant differences between the results with PW91 and PBE96. Although the surface energies obtained by Eq. (3) reveal slight oscillation as m increases, as noted in Ref. 44, the order and magnitude of surface energies are unchanged by using either Eq. (1) or (3).

B. 1-ethyl-3-methyl imidazolium tetrafluoroborate compounds

1. 1-ethyl-3-methyl imidazolium molecule

The EMIM ion is expressed as $[C_6H_{11}N_2]^{+1}$. The atomic numeration used in this paper is presented in Fig. 1. The hydrogen atoms are given the same number as the heavy atom they are bounded to, differentiation between ethyl and methyl hydrogen being unnecessary in this work. The EMIM ion and radical were optimized in a large $12\times10\times8$ Å^3 periodic box.

The relaxed bond lengths and bond angles are listed in Table II with other calculated results using molecular-orbital schemes.[14–16] The calculated total dipole moment of the molecule, taken at the center of the aromatic ring is 1.86D that compares well with $\mu=1.84$D (Ref. 14) and $\mu=1.76$D.[15] The bond distances for $EMIM^+$ are slightly larger than those of

TABLE I. PAW-PW91-GGA and PAW-PBE96-GGA (in parentheses) surface energies in mEh/a.u.^{2} (1 mEh/a.u.^{2} =0.097 17 eV/Å^2=1.5567 J/m^2) on Li (100), (110), and (111) surfaces. Results from Doll *et al.*[44] by the scheme of all-electron linear combination of Gaussian orbitals with PW91-GGA using 4*s*3*p* and 4*s*3*p*1*d* (in brackets) basis sets, and from Kokko *et al.*[45] by the norm conserving pseudopotential method with LDA, are also listed for comparison, the latter also report an experimental value of 0.30 mEh/a.u.^{2} for Li(110).

System	σ Eq. (1)	σ Eq. (3)	σ Eq. (2)[a]	σ Eq. (2)[b]
Li (100)	0.30	0.32	0.30	0.320
5 layers	(0.30)	n=6; m=1	[0.30]	
Li (100)	0.30			
6 layers	(0.30)			
Li (110)	0.31	0.29	0.32	0.345
5 layers	(0.31)	n=6; m=1	[0.32]	
Li (110)	0.32	0.33		
6 layers	(0.32)	n=7; m=1		
Li (110)	0.31	0.31		
7 layers	(0.31)	n=7; m=2		
Li (111)	0.34	0.31	0.34	0.395
5 layers	(0.34)	n=6; m=1	[0.36]	
Li (111)	0.35	0.37		
6 layers	(0.35)	n=7; m=1		
Li (111)	0.33	0.33		
7 layers	(0.33)	n=7; m=2		

[a]Reference 44.
[b]Reference 45.

Liu *et al.*[14] and de Andrade *et al.*,[15] and are in good agreement with those of Katsyuba *et al.*[16] The Hartree-Fock (HF) and DFT schemes produce substantially different results on bond lengths and binding energies as discussed by Lü *et al.*[17] It is natural that the results in Ref. 16 using the hybrid DFT (B3LYP, correct exchange, and GGA-like correlation) reveal better agreement with the present results. Generally, all calculated results are of the same order as those reported on EMIM-halide anion salts experiments.[46]

Table III lists the atomic charges on $EMIM^+$ and $EMIM^•$. The hydrogen values are included in heavier atoms that they are bounded to. Detailed values depend on the method of analysis due to inherent ambiguity of the definition of atomic charges. Orbital-based population analyses such as natural bond orbital (NBO) (Refs. 47 and 48) or Mulliken[49] are conceptually different from space analysis methods such as Voronoi[39–41] or the newly proposed Bader algorithm[50] used in plane-wave basis schemes. Recently, electrostatic-potential fit schemes such as a restrain electrostatic-potential (RESP) fit[51] or Merz-Singh-Kollman scheme[52,53] are often used. Our Voronoi results are in good agreement with RESP fit results except for those of N1, N2, and C4.

On the electronic structure, the $EMIM^•$-highest occupied molecular orbital (HOMO) is composed of pz (N1N2C3) with a small contribution of pz (C4C5) at −0.06 eV, and the lowest unoccupied molecular orbital (LUMO) lies at +0.22 eV. The second highest occupied orbital of $EMIM^•$ is composed of pz (C3C4C5)+εpz (N1N2) at −4.49 eV. By removing one electron, the latter becomes the HOMO of $EMIM^+$ at −0.17 eV, and the $EMIM^•$-HOMO becomes the LUMO of $EMIM^+$ at +4.78 eV, generating the gap of 4.95 eV. The remarkable contraction of C3-N distances when going from uncharged to charged EMIM can be explained by the component of the $EMIM^•$-HOMO of pz (N1N2C3).

2. Tetrafluoroborate molecule

The numeration of a BF_4 molecule used in this study is presented in Fig. 1. The ionic and radical molecules were optimized in a large 8×8×8 Å^3 box. The B-F mean distance in BF_4^- is 1.422 Å compared to 1.418 Å [B3LYP/6-31+G(*d*,*p*) (Ref. 17)], 1.397 Å [HF/6-31+G(*d*,*p*) (Ref. 17) and HF/6-31G(*d*) (Ref. 14)], and 1.389 Å [exp. for $NaBF_4$ (Ref. 54)]. The better agreement with that obtained by the hybrid DFT is reasonable. The atomic charge results are listed in Table IV together with other theoretical results.[15,17–20] Our results are more close to the electrostatic-potential fit results than the NBO results.

For $BF_4^•$, the HOMO for up spin and the LUMO for down spin are composed mainly of degenerated 2 pz(F2F3+F4F5) with a smaller px+py(F) contribution and 1 py(F2F3)+px(F4F5) with each equal occupation. The LUMO for up spin is composed of s(BF) (+9.40 eV) as the second lowest unoccupied orbital for down spin. For BF_4^-, the LUMO is mainly composed of s(BF) at +5.47 eV, and the degenerated HOMO is composed of pz(F) and smaller px(F)+py(F) at −0.17 eV. Interestingly, the HOMO-LUMO gap for up spin in $BF_4^•$ over 9 eV is greatly reduced to 5.63 eV for the HOMO-LUMO gap of BF_4^-.

3. 1-ethyl-3-methyl imidazolium tetrafluoroborate pair

Figure 1 presents the optimized configuration of the EMIM-BF_4 molecular pair obtained by a 16×16×16 Å^3

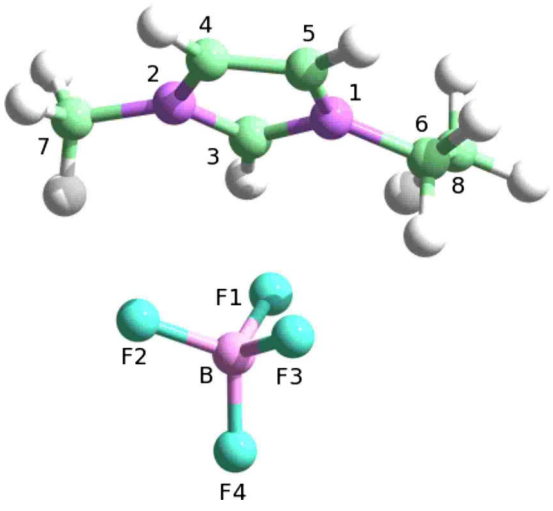

FIG. 1. (Color online) Representation of EMIM-BF_4 molecular pair. Note that hydrogen atoms are given the same number as the heavy atom they are bounded to.

TABLE II. Geometric details of $EMIM^+$ optimized by PAW-PW91-GGA, compared to other $EMIM^+$ results using molecular-orbital schemes (Refs. 14–16) and x-ray experiments (Ref. 46). $EMIM^•$ radical results are also listed for comparison. All distances are in angstrom and angles are in degree.

Type	Index	$EMIM^+$	$EMIM^•$	14[a]	15[b]	16[c]	46[d]	46[e]
C-N	2–3	1.343	1.385	1.316	1.317	N/A	1.368	1.369
	1–3	1.343	1.386	1.315	1.314	1.335	1.327	1.324
	2–4	1.382	1.383	1.378	1.377	1.385	1.367	1.368
	1–5	1.381	1.388	1.378	1.377	1.385	1.376	1.374
	2–7	1.467	1.444	1.466	1.469	1.467	1.449	1.462
	1–6	1.479	1.451	1.478	1.477	1.480	1.489	1.475
C-C	4–5	1.368	1.365	1.343	1.342	1.363	1.352	1.322
	6–8	1.522	1.525	N/A	1.522	1.527	1.472	1.475

Type	Index	$EMIM^+$	$EMIM^•$	15[b]	16[c]	46[d]	46[e]
N-C-C	1–5–4	107.120	108.125	107.1	107.2	106.5	107.4
N-C-C	2–4–5	107.159	108.243	107.1	106.9	107.4	107.7
C-N-C	3–1–5	108.525	108.126	108.0	108.5	108.8	107.7
C-N-C	3–2–7	125.457	124.740	125.8	123.9	125.0	123.8
C-N-C	6–1–5	125.556	126.068	125.8	127.0	125.3	126.4
C-C-N	8–6–1	110.460	112.445	112.1	111.3	111.6	111.5

[a]RHF/6-31+G(*d*).
[b]UHF/6-31G(*d*).
[c]B3LYP/6-31G*.
[d]Exp. for EMIM-Br.
[e]Exp. for EMIM-I.

box. The detailed bond lengths and bond angles are listed in Table V. The structure of each constituent molecule is slightly changed from each isolated charged system by mutual interactions. The B-F distances change to 1.431, 1.437, 1.439, and 1.388 Å from the value of 1.422 Å. The structure of $EMIM^+$ shows only small perturbation: the average change for N-C distances is ~0.001 Å, which for C-C distances is ~0.003 Å and that for C-H distances is less than 0.001 Å.

On the relative position of the two constituent molecules, F1 is close to H3, F2 is close to H7, and F3 is close to H6. The closest distance between BF_4 and EMIM, namely the F1-H3 distance, is 2.061 Å while setting an initial geometry with F1 and H3 too close to each other results in a pseudominimum at 1.864 Å. The minimum reported in Ref. 18 and possibly in Ref. 15 corresponds to a configuration where two F atoms of BF_4^- contact with H3 of $EMIM^+$. References 14, 21, and 16 present however the minimum with only small differences from the present results. The better agreement with Refs. 21 and 16 using the hybrid DFT for the intermolecular distances is reasonable.

The binding energy, taken as the difference of the optimized energy of EMIM-BF_4 pair and the energy of $EMIM^+$ and BF_4^- ions, is −3.619 eV (349.18 kJ/mol; 83.45 kcal/mol) which compares well with other theoretical results: 345.6 kJ/mol [RHF/6-31+G(*d*), Ref. 14], 353.5 kJ/mol [B3LYP/6-31+G(*d*,*p*), Ref. 17], 350.5 kJ/mol [HF/6-31+G(*d*,*p*), Ref. 17], 344.96 kJ/mol [B3LYP/6-31++G(*d*,*p*), Ref. 19], and 85.2 kcal/mol (MP2/6-311G**//HF/6-311G, Ref. 18).

The charge transfer from BF_4^- to $EMIM^+$ is of 0.275*e* by the Voronoi decomposition, as compared to 0.043 in Ref. 18. The HOMO-LUMO gap of [EMIM][BF_4] is 4.82 eV. The HOMO of [EMIM][BF_4] is similar to the HOMO of the isolated BF_4^- and is composed of *py*(F2F3F1)+*px*(F3F1), which is quasidegenerated with the lower *py*(F3F4F1)+*pz*(F2F3F1). The LUMO of [EMIM][BF_4] is composed of *px*(C3N2N1)+*pz*(C3N2N1) similar to the LUMO of the

TABLE III. Formal atomic charges (in electrons) of optimized $EMIM^+$ and $EMIM^•$ compared to other theoretical results of $EMIM^+$ using molecular-orbital schemes (Refs. 14, 15, and 18). Charge values on hydrogen atoms are included to the values of carbon atoms that they are bounded to.

q	$EMIM^+$	$EMIM^•$	18[a]	14[b]	15[c]
N1	−0.055	−0.106	+0.06	+0.0095	−0.0100
N2	−0.044	−0.106	+0.28	+0.0618	+0.0795
C3	+0.278	+0.078	+0.10	+0.2402	+0.2627
C4	+0.225	+0.087	+0.03	+0.0967	+0.0811
C5	+0.097	+0.017	+0.09	+0.0522	+0.0662
C6	+0.201	+0.084	+0.23	+0.2046	+0.2112
C7	+0.232	+0.032	+0.16	+0.2420	+0.2222
C8	+0.061	−0.085	+0.06	+0.0930	+0.0873

[a]Merz-Shing-Kollman scheme (Refs. 52 and 53), MP2/6-311G**//HF/6-311G.
[b]RESP fit (Ref. 51) RHF/6-31+G(*d*).
[c]RESP fit (Ref. 51) UHF/6-31G(*d*).

TABLE IV. Formal atomic charges (in electrons) of optimized BF_4^- and $BF_4^\bullet$, compared to other theoretical results of BF_4^- using molecular-orbital schemes (Refs. 15 and 17–20).

q	BF_4^-	$BF_4^\bullet$	18	19[a]	15	20[b]	17[c,d]
B	0.976	0.955	0.92	1.56	0.8275	0.9756	1.579(1.435)
F	−0.494	−0.239	−0.48	−0.61	−0.4569	−0.4939	−0.645(−0.609)

[a]NBO (Refs. 47 and 48), B3LYP/6-31++G(d,p).
[b]RESP fit (Ref. 51), HF/6-31G**.
[c]NBO, HF/6-31+G(d,p).
[d]NBO, B3LYP/6-31+G(d,p).

isolated $EMIM^+$. The density of states (DOS) of the EMIM-BF_4 pair is almost a simple superposition of the DOSs of the two isolated charged systems although the relative positions of the states in the two systems in the energy axis should depend on the charge transfer and electrostatic interactions. The state corresponding to the HOMO of $EMIM^+$ is located just below the HOMO of BF_4^- in the pair configuration, resulting in the reduction in the HOMO-LUMO gap from 4.95 eV in the isolated $EMIM^+$ to 4.82 eV.

C. 1-ethyl-3-methyl imidazolium tetrafluoroborate molecular-pair adsorption

1. Supercells

For the adsorption of the EMIM-BF_4 pair, a large 4×4 Li-surface cell was taken. For side-on configurations where the EMIM-BF_4 molecule is adsorbed parallel to the surface, the minimum distance between the adsorbates is 6.3, 6.3, and 12.3 Å for (100), (110), and (111) surfaces, respectively. As for the Li slab, we used a five-layer slab with fixed bottom two layers. The period in the z coordinate was 20, 30, and 20 Å for Li (100), (110), and (111) surfaces, respectively, leading to a minimum distance between EMIM-BF_4 and the replicated bottom Li layer of about 8, 14, and 10 Å in the side-on configuration. The adsorption energy is defined as follows:

$$E_{\text{ads}} = E_{\text{final}} - \sum E_{\text{reactants}}, \tag{4}$$

where the second term is the sum of energies of the relaxed $p4\times4$ Li clean surface and the isolated EMIM-BF_4 pair. Here the Li-BF_4 molecule was examined in a $14\times14\times14$ $Å^3$ cell by the present scheme for the analysis of the Li-BF_4 interactions.

Several adsorption configurations have been examined for each Li surface. An initial configuration is constructed by setting the optimized EMIM-BF_4 pair (Fig. 1) on a Li surface and is relaxed. On the orientation of the molecular pair on the Li surface, we consider the side-on and end-on modes. In the latter, EMIM-BF_4 is adsorbed perpendicular to the surface. For the side-on mode, we deal with two coordination modes: the on-top mode (BF_4 is linked to one surface atom) and the bridge mode (BF_4 contacts with two neighboring surface atoms). For the side-on mode, the ethyl group was directed either outward the surface or toward the surface. The latter is called reversed mode.

2. (100) side-on on-top adsorption

In the relaxed configuration, a Li atom contacting with BF_4 is attracted toward BF_4, leading to an increase in its z-axis height of about 0.41 Å, as can be seen in Fig. 2(a). On the other hand, the EMIM group is repelled to an almost horizontal position. The distance between this Li atom and F is 1.851 Å as compared to 1.816 Å in the Li-BF_4 molecule with the corresponding B-F distance being stretched to 1.479 Å, and the other B-F distances being 1.383, 1.413, and 1.416 Å as compared to 1.493 and 1.368 Å in the Li-BF_4 molecule. The three shortest F-H distances at the interface between EMIM and BF_4 are now 2.047, 2.291, and 2.456 Å, as compared with those (2.061, 2.168, and 2.385 Å) of the [EMIM][BF_4] system in Table V, which indicates no serious changes of the interfacial configuration between EMIM and BF_4 in the adsorption. The isosurface and contour plot of charge density (Fig. 2) show charge-density depletion under the attracted Li atom, which could, with a subsequent perturbation of the surface, lead to its removal from the surface, eventually forming a free Li-BF_4 species.

The adsorption energy E_{ads} is −0.938 eV (−90.5 kJ/mol; −21.6 kcal/mol). The electron transfer is evaluated to $0.572e$ from the Li surface to the molecular pair by the Voronoi decomposition. The total charge on BF_4 slightly increases from $-0.726e$ in the isolated [EMIM][BF_4] pair to $-0.755e$. It is $-0.679e$ in the Li-BF_4 molecule. The striking change is observed in the total charge on EMIM, which decreases from $+0.725e$ to $+0.183e$ via the attraction of 0.542 electrons, thus being more close to $EMIM^\bullet$.

In Fig. 3, the LDOS of the attracted Li atom shows hybridization with BF_4 molecular states. The HOMO-LUMO gap of the [EMIM][BF_4] part is now covered by the Li metallic states, and the metallic Fermi level is located inside the HOMO-LUMO gap. This kind of feature is similar to that of metal/semiconductor interfaces.[27,28] The features of the LDOSs of the [EMIM][BF_4] part are not so greatly changed from those of the isolated molecular pair. The noticeable change is the relative higher shift of the EMIM-DOS or the lower shift of the BF_4-DOS. The highest occupied state of the [EMIM][BF_4] part is that of $EMIM^+$ in Fig. 3 although the HOMO of the isolated [EMIM][BF_4] is the BF_4^- state. This reversion is also observed in the increase in the energy difference between the bottom states of BF_4^- and $EMIM^+$ in Fig. 3. This should be caused by the electron transfer to $EMIM^+$. In Fig. 3, the Fermi level is located below the LUMO-like peak of the [EMIM][BF_4] part. This point indi-

TABLE V. Geometric details of the optimized EMIM-BF_4 molecular pair, compared to other theoretical results using molecular-orbital schemes (Refs. 14, 16–18, and 21). The number in ⟨ ⟩ indicates the average on all corresponding H atoms. Distances are in angstrom and angles are in degree.

Type	Index	Pair	Isolated ion	18[a]	14[b]	21[c]	16[d]	17[e]	17[f]
C-N	2–3	1.342	1.343	1.312	N/A	N/A	N/A	N/A	N/A
	1–3	1.341	1.343	1.313					
	2–4	1.384	1.382	1.379					
	1–5	1.383	1.381	1.380					
	2–7	1.467	1.467	1.463					
	1–6	1.480	1.479	1.472					
C-C	4–5	1.366	1.368	1.338	N/A	N/A	N/A	N/A	N/A
	6–8	1.519	1.522	1.522					
C-H	3–3	1.089	1.082	1.067	N/A	N/A	N/A	N/A	N/A
	4–4	1.082	1.082	1.068					
	5–5	1.081	1.082	1.067					
	6–⟨6⟩	1.095	1.097	1.081					
	7–⟨7⟩	1.095	1.093	1.080					
	8–⟨8⟩	1.097	1.098	1.084					
B-F	B-F1	1.431	1.422	1.400	N/A	N/A	N/A	1.401	1.421
	B-F2	1.437	1.422	1.408				1.410	1.431
	B-F3	1.439	1.422	1.412				1.409	1.437
	B-F4	1.388	1.422	1.355				1.360	1.377
BF-HC	F1-H3	2.061		2.12	2.11	2.061	2.030	2.197	2.258
	F2-H7	2.168		2.25	2.44	2.228	2.230	2.343	2.226
	F3-H6	2.385		2.65	2.64	2.460	N/A	2.552	2.506

Angle type	Index	[EMIM-BF_4]	$EMIM^+$	18[a]
N-C-C	1–5–4	107.118	107.120	107.056
N-C-C	2–4–5	106.913	107.159	107.031
C-N-C	3–1–5	108.803	108.525	108.032
C-N-C	3–2–7	124.182	125.457	125.018
C-N-C	6–1–5	125.626	125.556	126.526
C-C-N	8–6–1	112.975	110.460	111.753

[a]HF/6-311G**, from supplementary material of Ref. 18, also reporting C3-H3…B=2.46 Å, which is 2.435 Å in our results.
[b]RHF/6-31+G(*d*).
[c]B3LYP/6-311+G(2*d*,*p*).
[d]B3LYP/6-31+G*.
[e]HF/6-31+G(*d*,*p*).
[f]B3LYP/6-31+G(*d*,*p*).

cates no substantial reduction in $EMIM^+$ in the viewpoint of orbital occupation, in spite of the evaluated electron transfer to $EMIM^+$. This paradox will be discussed later.

3. (100) end-on adsorption

This adsorption mode was examined in order to see the difference when EMIM group does not directly contact with the Li surface. A 30-Å-height periodic box was taken to deal with this system. As shown in Fig. 4, the Li atom under BF_4 is still attracted toward BF_4, leading to an increase in its height of about 0.36 Å, which is a little smaller than that in the side-on on-top case. The distance between this Li atom and F is 1.857 Å (1.816 Å in Li-BF_4), the corresponding B-F distance being stretched to 1.448 Å, the other B-F distances being 1.397, 1.417, and 1.422 Å (1.493 and 1.368 Å in Li-BF_4). The three shortest F-H distances between EMIM and BF_4 are now 2.005, 2.253, and 2.412 Å, as compared with those (2.061, 2.168, and 2.385 Å) in the [EMIM][BF_4] system. The isosurface and contour plot of charge density in Fig. 4 also show charge-density depletion under the attracted Li atom, which could lead to its removal from the surface. However this perturbation seems to be less significant than in the side-on on-top case.

The adsorption energy E_{ads} is −0.598 eV (−57.7 kJ/mol; −13.8 kcal/mol), which is about 64% of that of the side-on on-top case. The charge transfer between the surface and

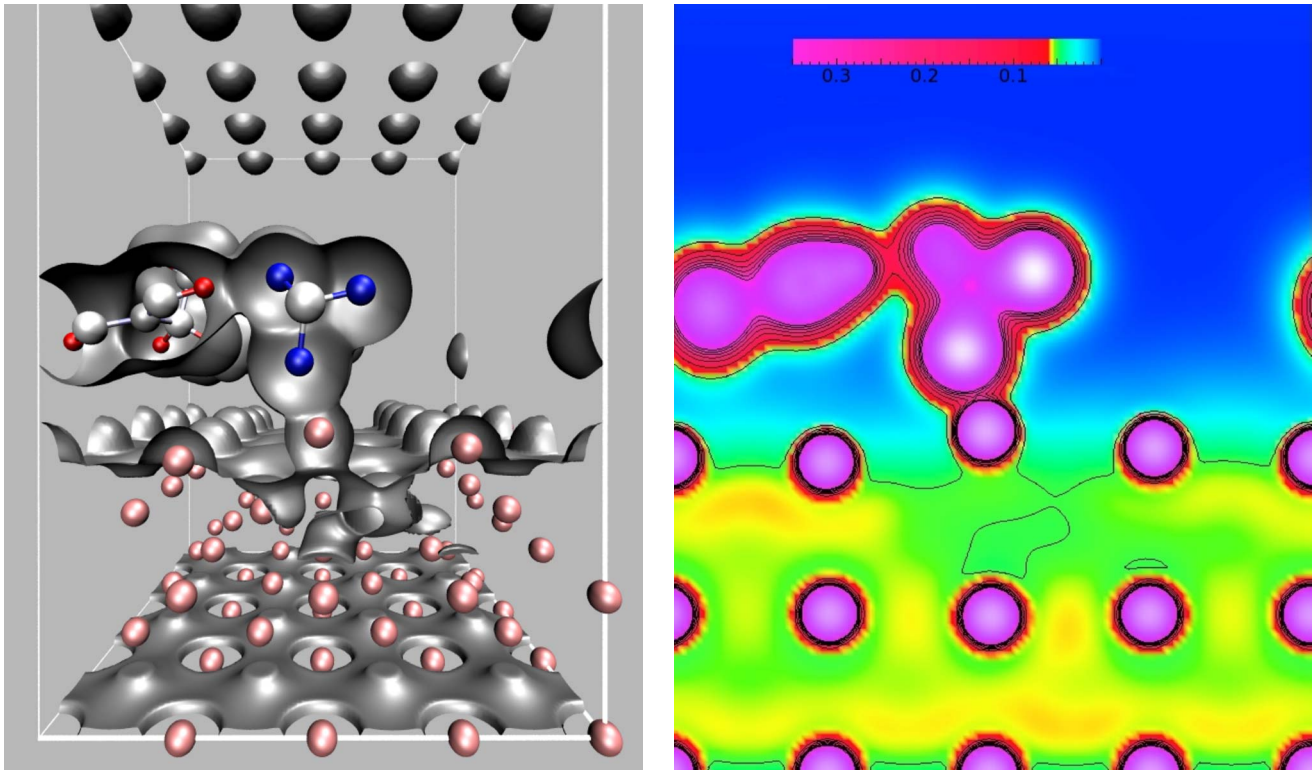

FIG. 2. (Color online) Valence-electron charge density for EMIM-BF_4 side-on on-top adsorption onto a Li (100) surface. (a) Isosurface of $0.05e/Å^3$, and (b) cross-sectional contour plot with concentric $0.05e/Å^3$ lines and an abrupt change in color at $0.05e/Å^3$, which clarifies that the charge-density change is localized under the attracted Li atom.

[EMIM][BF_4] is evaluated to $0.185e$ within the Voronoi distribution, which is about 32% of that of the side-on on-top case. The total charge on BF_4 slightly increases from $-0.726e$ to $-0.769e$, and that on EMIM decreases from $+0.725e$ to $+0.584e$. The latter means that the electron transfer toward $EMIM^+$ is greatly reduced to $0.141e$ as compared with $0.542e$ in the side-on on-top case.

In Fig. 5, the LDOS of the attracted Li atom reveals hybridization with BF_4 molecular states similarly to the side-on on-top case. The Fermi level is located inside the HOMO-LUMO gap of the [EMIM][BF_4] part although it lies just below the states corresponding to the LUMO. The present Fermi level measured from the state corresponding to the HOMO of [EMIM][BF_4] is about 5 eV, which is a little larger than that in the side-on case, about 4.2 eV in Fig. 3. This relation is consistent with the larger charge transfer from the metal side in the side-on case, which causes larger interface dipole to lower the electrostatic potential in the metal side relatively, resulting in the lower Fermi level in the HOMO-LUMO gap in the side-on case. This is consistent with the behavior of the Schottky-barrier heights at metal/oxide interfaces[55] where the interface charge transfer dominates the connecting position of the metal Fermi level via the interface dipole. The higher shift of the EMIM-DOS is less significant in the present case than in the side-on case due to relatively small charge transfer toward $EMIM^+$.

4. (110) side-on bridge adsorption

Figure 6 shows the bridge-site adsorption on the (110) surface of the side-on mode, where two F atoms are linked to two Li atoms, the B-F distances being at 1.447 and 1.499 Å (1.493 Å in Li-BF_4), and the other two B-F being at 1.371 and 1.383 Å (1.368 Å in Li-BF_4). For the attracted Li atoms, the mean height increase is 0.98 Å compared to 0.41 Å in the (100) side-on on-top adsorption. The isosurface and contour plot of charge density in Fig. 6 show the

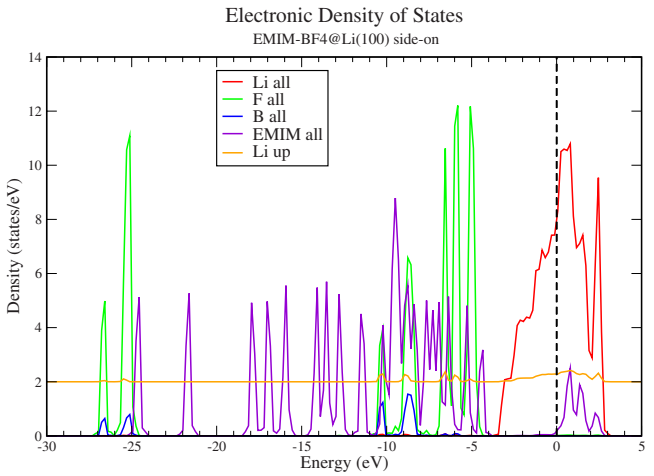

FIG. 3. (Color online) Electronic density of states for EMIM-BF_4 side-on on-top adsorption onto a Li (100) surface. Origin of the energy axis is taken at the Fermi level. "Li all" stands for all Li contributions, and "Li up" indicates the LDOS of the attracted Li atom, which is shifted to 2 states/eV and multiplied by five in order to have a better sight.

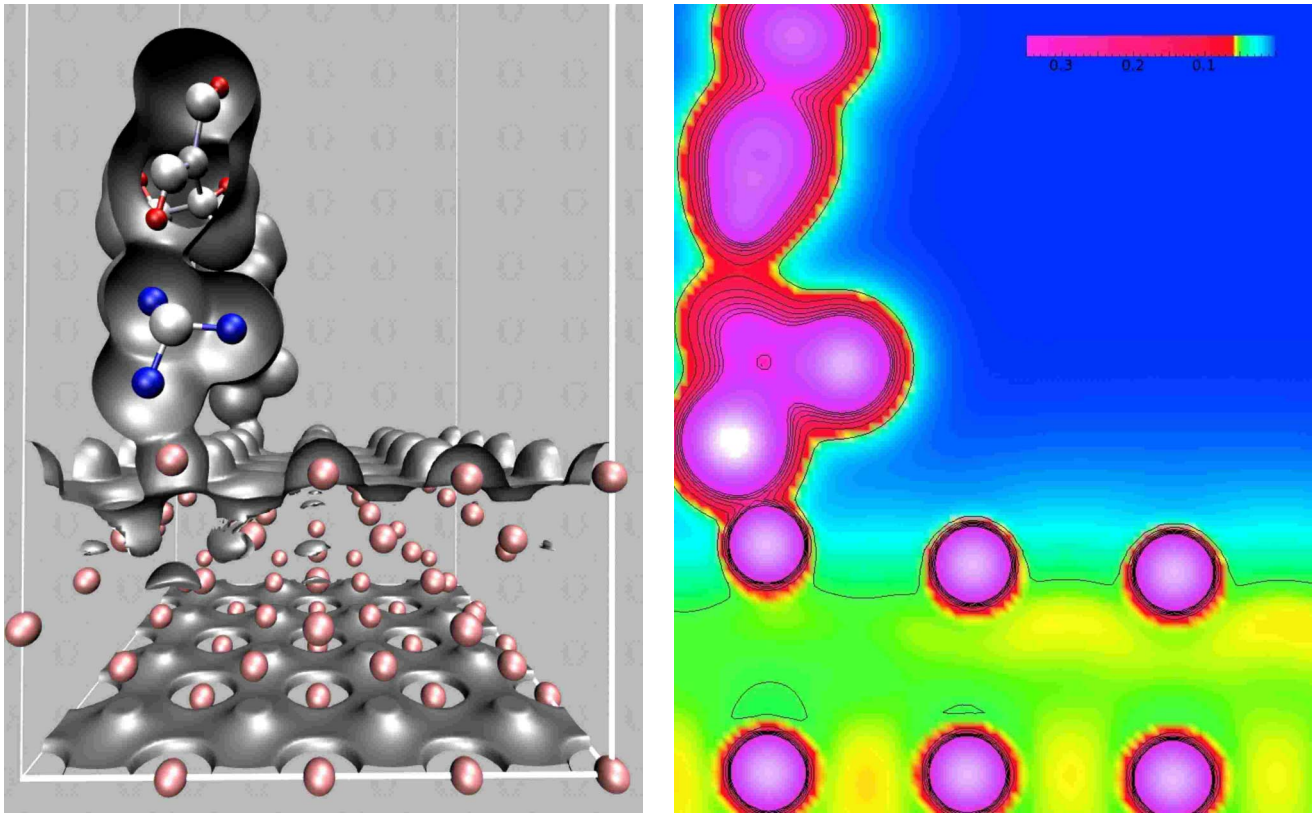

FIG. 4. (Color online) Valence-electron charge density for EMIM-BF_4 end-on adsorption onto a Li (100) surface. (a) Isosurface of $0.05e/Å^3$, and (b) cross-sectional contour plot with concentric $0.05e/Å^3$ lines and an abrupt change in color at $0.05e/Å^3$.

charge depletion region under the attracted Li atoms.

The adsorption energy E_{ads} is −1.327 eV (−128 kJ/mol; −30.6 kcal/mol), and the charge transfer between the surface and [EMIM][BF_4] is evaluated to $0.615e$ within the Voronoi distribution. Both quantities are larger than those in the preceding examples of the adsorptions on the (100) surface due to a larger number of atoms involved in direct contact. The total charge on BF_4 slightly decreases from $-0.726e$ to $-0.640e$ while that on EMIM seriously decreases from $+0.725e$ to $+0.025e$ by the attraction of 0.70 electrons, thus being more close to $EMIM^{\bullet}$ charge.

In Fig. 7, the LDOS of the attracted Li atoms shows remarkable hybridization with BF_4 molecular states. We can also see that the third peak from the top in the BF_4-DOS is split into two smaller peaks owing to the stronger Li-F interactions in the present system. As adsorptions on the (100) surface (Figs. 3 and 5), the Fermi level is located inside the HOMO-LUMO gap of the [EMIM][BF_4] part. The Fermi level measured from the state corresponding to the HOMO of [EMIM][BF_4] is about 4 eV, which is smaller than the adsorptions on the (100) surface, 4.2 and 5 eV. As discussed above, this is caused by the larger electron transfer from the metal side to $EMIM^+$, generating larger interface dipole, and leading to the relative higher shift of the EMIM-DOS against the Fermi level. Note that BF_4 does not gain electrons, which also enhances the higher shift of the EMIM-DOS against the BF_4-DOS.

Incidentally, the higher shift of the EMIM-DOS should make the occupation of the LUMO-like states of $EMIM^+$ difficult, which might paradoxically prevent the reduction in $EMIM^+$ or the electron transfer to $EMIM^+$ as pointed out above. However, in Fig. 7, a DOS-tail with slight occupancy at the Fermi level is generated below the sharp peaks corresponding to the EMIM-LUMO-like states, caused by the hybridization with Li metallic states. This should be concerned

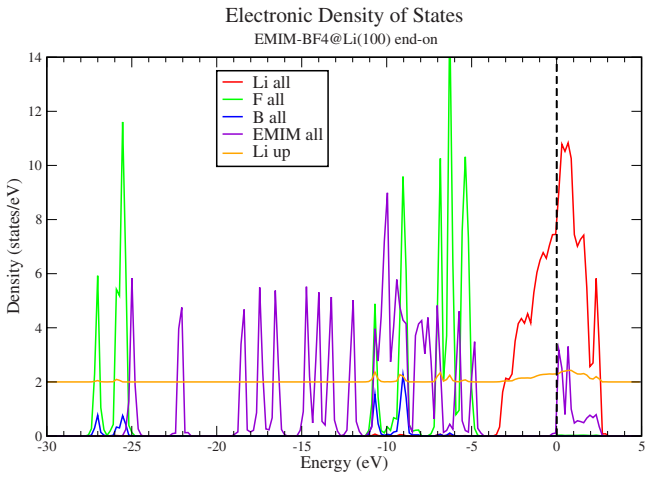

FIG. 5. (Color online) Electronic density of states for EMIM-BF_4 end-on adsorption onto a Li (100) surface. Origin of the energy axis is taken at the Fermi level. "Li all" stands for all Li contributions. "Li up" indicates the LDOS of the attracted Li atom, which is shifted to 2 states/eV and multiplied by five for a better view.

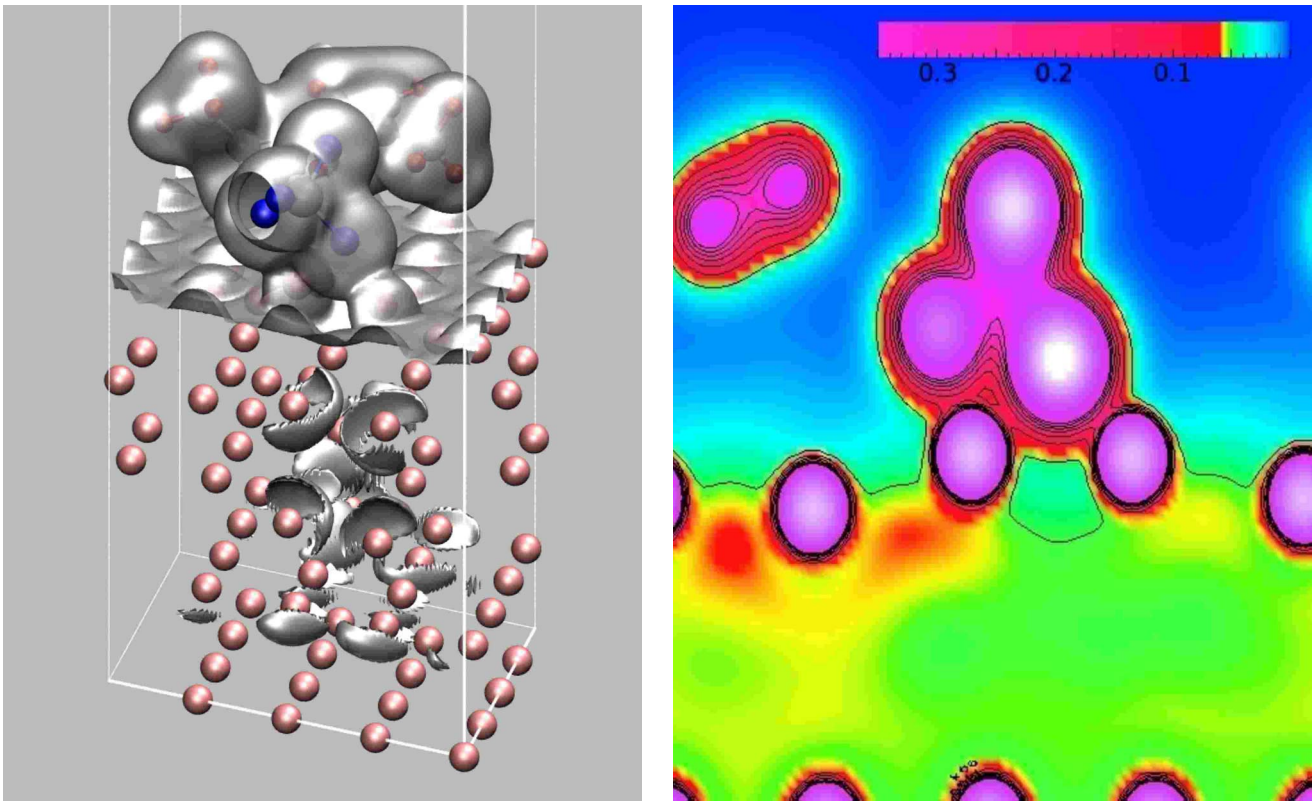

FIG. 6. (Color online) Charge density for EMIM-BF_4 side-on bridge adsorption onto a Li (110) surface. (a) Isosurface of $0.05e/Å^3$, and (b) cross-sectional contour plot with concentric $0.05e/Å^3$ lines and an abrupt change in color at $0.05e/Å^3$.

with the partial reduction in $EMIM^+$ or the electron transfer, as discussed later.

5. Side-on on-top adsorption on gold (100)

In order to examine whether the present results are typical of Li surfaces or not, we performed similar computations of the side-on on-top adsorption of EMIM-BF_4 on a Au (100) surface. Using the optimized lattice parameter of fcc Au, we obtained the relaxed configuration as shown in Fig. 8. The Au atoms under BF_4 are not displaced toward BF_4. The shortest Au-F distance is 2.655 Å as compared with 1.851 Å for the Li-F distance in the Li (100) case. The perturbation in the EMIM-BF_4 configuration is quite small. The isosurface and contour plot of charge density show no clear charge depletion in the Au side under the BF_4 molecule except for only local perturbation of the charge density at the contact region.

The adsorption energy E_{ads} is −0.440 eV (−42.45 kJ/mol; −10.15 kcal/mol), which is less than half of that of the Li (100) case. The charge transfer between the surface and [EMIM][BF_4] is evaluated to $0.739e$ within the Voronoi analysis. The total charge on BF_4 increases from $-0.726e$ to $-0.957e$, and that on EMIM decreases from $+0.725e$ to $+0.218e$. This means that both BF_4 and EMIM gain the electrons substantially in the adsorption, which is quite different from the Li cases.

In Fig. 9, the Fermi level now lies in the midpoint of the HOMO-LUMO gap of the [EMIM][BF_4] part. The Fermi level measured from the HOMO of the [EMIM][BF_4] part is 2.5 eV, which is much smaller than the Li cases, 4.2, 5, and 4 eV in Figs. 3, 5, and 7. In the Li cases, the larger charge transfer makes this energy difference smaller. Indeed the evaluated transfer value ($0.739e$) is larger than the Li cases. Of course, the problem of the band continuity between two

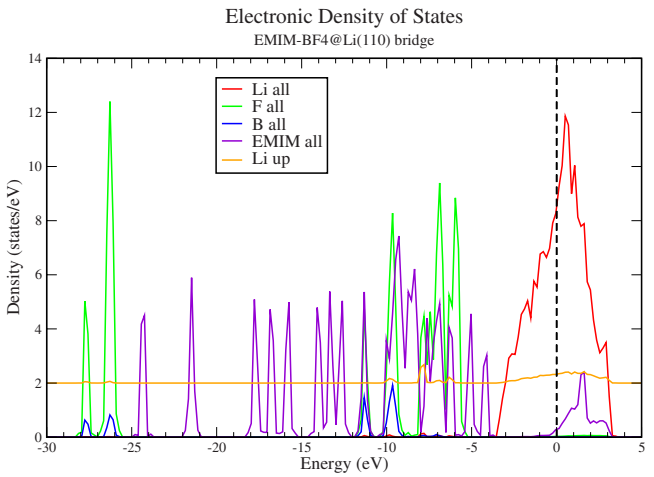

FIG. 7. (Color online) Electronic density of states for EMIM-BF_4 side-on bridge adsorption onto a Li (110) surface. Origin of the energy axis is taken at the Fermi level. "Li all" stands for all Li contributions and "Li up" indicates the LDOS of the attracted Li atoms, which is shifted to 2 states/eV and multiplied by five.

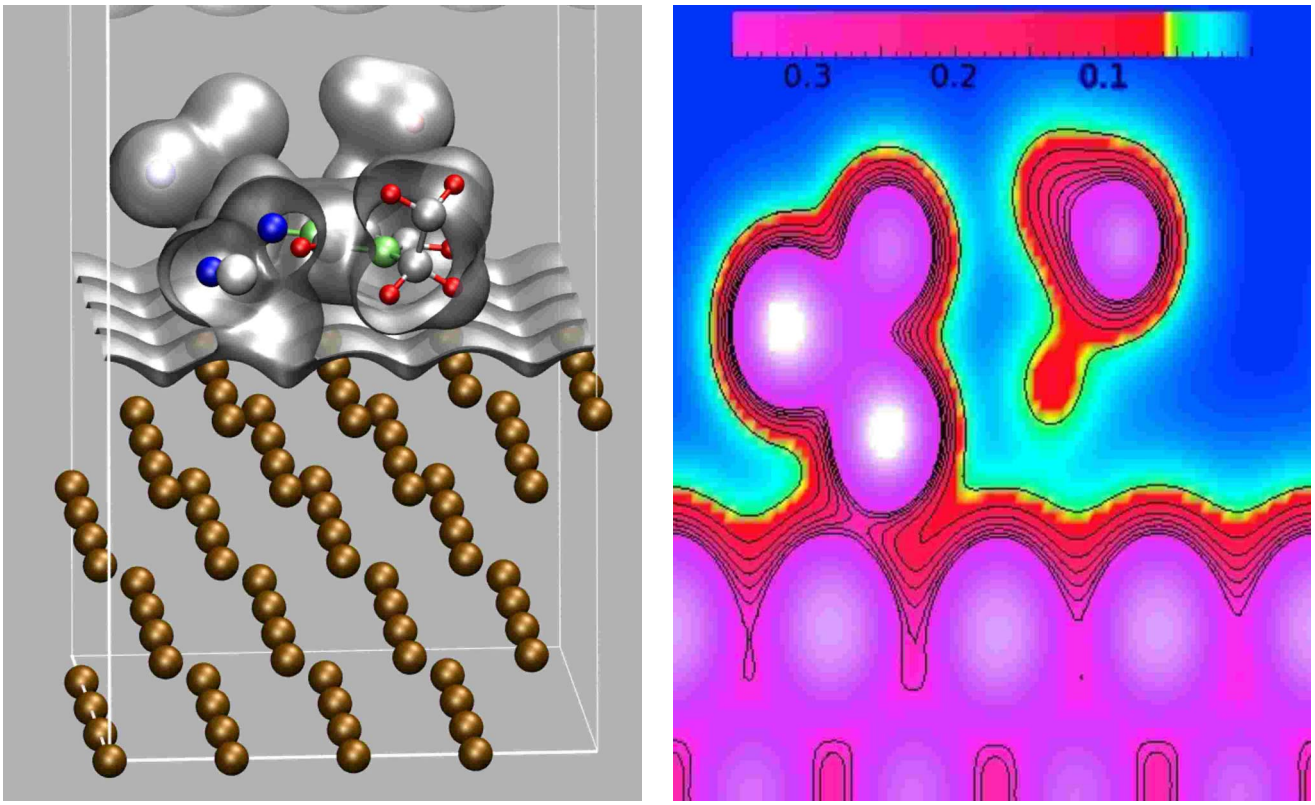

FIG. 8. (Color online) Charge density for EMIM-BF_4 side-on on-top adsorption onto a Au (100) surface. (a) Isosurface of $0.05e/\text{Å}^3$, and (b) cross-sectional contour plot with concentric $0.05e/\text{Å}^3$ lines and an abrupt change in color at $0.05e/\text{Å}^3$.

materials depends on the relation of the intrinsic electronic structures of the two materials in addition to the interface dipole,[55] and thus simple comparison with the Li cases is not meaningful.

On the other hand, the peak corresponding to the HOMO of $EMIM^+$ is located near the peak corresponding to the HOMO of BF_4^-, indicating no higher relative shift of the EMIM-DOS against the BF_4-DOS in spite of the substantial charge transfer to $EMIM^+$, quite differently from the Li cases. This point seems to be concerned with the fact that both BF_4 and EMIM gain electrons and that the charge transfer may have different nature in the Au-surface case, as analyzed later.

6. Other surfaces and adsorption modes

All the results of examined adsorption configurations on Li surfaces are listed in Table VI as well as one example of the Au-surface adsorption. For the side-on adsorptions on Li, regardless of the coordination modes or surfaces, we observed the following general features: (1) large displacements of one or two Li atoms toward BF_4^-, generating charge-density depletion region under the Li atoms, (2) charge transfer of about $0.5e-0.7e$ from the surface to EMIM-BF_4, (3) an electronic gain of about $0.5e-0.7e$ for $EMIM^+$ and a relative stable electronic charge for BF_4^-, and (4) the adsorption energy of about 0.8–1.5 eV.

For the end-on adsorption compared to the side-on adsorptions, the adsorption energy is about half and the charge transfer is quite low. At least for the case of molecular-pair adsorption, end-on adsorptions with less energy gain seem unlikely to occur spontaneously. The side-on bridge adsorptions are the most favored for each Li surface, due to the increased number of Li-surface atoms involved. For the adsorption on a Au (100) surface, the adsorption energy is less

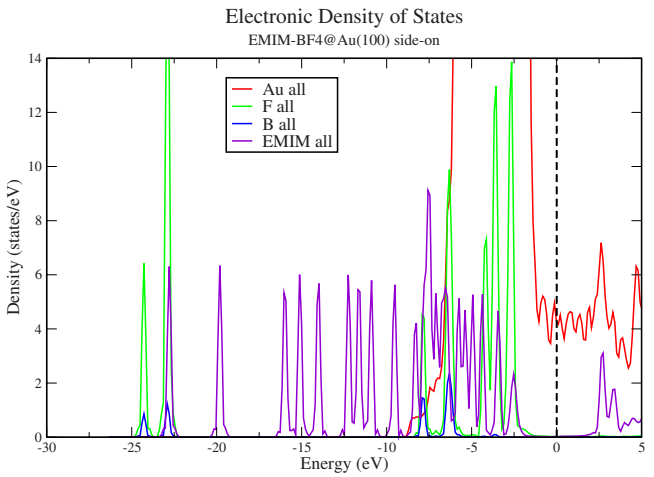

FIG. 9. (Color online) Electronic density of states for EMIM-BF_4 side-on on-top adsorption onto a Au (100) surface. Origin of the energy axis is taken at the Fermi level. "Au all" stands for all gold contributions, and was scaled down to a quarter of its intensity value.

TABLE VI. Results on EMIM-BF_4 adsorptions onto Li (100), (110), and (111) surfaces with different adsorption modes. The adsorption energy E_{ads}, the interfacial charge transfer q, the BF_4 and EMIM charges, the charge differences for BF_4 and EMIM (with respect to the [EMIM][BF_4] pair), the mean height change of attracted Li atoms Δz_{Li}, and the minimum Li-F distances are listed. *R* indicates the reversed side-on configurations with respect to the direction of the ethyl group against the surface. Gold indicates the side-on on-top adsorption on a Au (100) surface.

Surface	(100)						(110)				(111)			
Mode	On-top	On-top (*R*)	Bridge	Bridge (*R*)	End-on	Gold	On-top	On-top (*R*)	Bridge	Bridge (*R*)	On-top	On-top (*R*)	Bridge	Bridge (*R*)
E_{ads}(eV)	−0.938	−0.887	−1.320	−1.056	−0.598	−0.440	−0.891	−0.995	−1.327	−1.208	−0.881	−0.809	−1.452	−1.255
$q(e)$	0.572	0.718	0.586	0.662	0.185	0.739	0.686	0.510	0.615	0.511	0.570	0.480	0.551	0.550
$q$$BF_4$	−0.755	−0.777	−0.714	−0.738	−0.769	−0.957	−0.704	−0.629	−0.640	−0.600	−0.688	−0.722	−0.677	−0.712
$\Delta q$$BF_4$	0.030	0.052	−0.011	0.013	0.044	0.232	−0.021	−0.096	−0.085	−0.125	−0.037	−0.003	−0.048	−0.013
qEMIM	0.183	0.059	0.128	0.076	0.584	0.218	0.018	0.119	0.025	0.089	0.188	0.242	0.126	0.163
ΔqEMIM	0.542	0.666	0.597	0.649	0.141	0.507	0.707	0.606	0.700	0.636	0.537	0.483	0.599	0.562
Δz_{Li}(Å) [a]	0.41	0.45	0.51	0.28	0.36	0.05	1.26	0.62	0.98	0.78	0.50	0.46	0.44	0.50
Li-F[a]	1.851	2.001	1.886	1.951	1.857	2.655	1.965	1.99 1	1.912	1.980	1.831	1.854	1.898	1.882

[a]When two Li atoms are attracted, the mean value is presented.

than half of those in the Li-surface cases. The striking difference is no substantial displacement of surface Au atoms under the molecule. The total charge transfer is in a similar range although the changes in the charge of each molecular unit are quite different. The charge of BF_4 is substantially increased.

D. Discussion

In the LDOSs of the EMIM-BF_4/Li systems, we can see the following tendency: the larger electron gain for $EMIM^+$ from the Li surface and the less electron gain or larger loss for BF_4^- cause the higher relative shift of the EMIM-DOS against the BF_4-DOS, resulting in a smaller energy difference between the HOMO of the [EMIM][BF_4] part and the metallic Fermi level. This feature is most remarkable in the (110) side-on bridge adsorption (Fig. 7). However, this tendency causes a paradoxical problem. For the system with larger electron gain for $EMIM^+$, the location of the DOS peak corresponding to the $EMIM^+$-LUMO also becomes much higher from the Fermi level, which should result in a negligible occupancy of the states corresponding to the $EMIM^+$-LUMO. This implies a question whether the electron transfer toward $EMIM^+$ could mean substantial chemical reduction in $EMIM^+$, namely, the formation of $EMIM^•$ radical, or not.

On the other hand, in Figs. 3 and 7, we can see the presence of tails of DOS below the large sharp peak corresponding to the $EMIM^+$-LUMO, resulting in a small occupancy of the EMIM-DOS at the Fermi level, as can be seen remarkably in Fig. 7. Such tails should be caused by the hybridization between the $EMIM^+$-LUMO-like states and the Li metallic states, and may be concerned with the charge transfer to $EMIM^+$. In any case, detailed analysis of the charge transfer to $EMIM^+$ is essential.

In the LDOSs of the adsorption on a Au surface (Fig. 9), there also exists one paradoxical problem as mentioned above. There is no significant relative shift of the EMIM-DOS against the BF_4-DOS in the LDOSs, indicating no large charge (electron) transfer from the Au surface toward $EMIM^+$. But the calculated transfer value itself is not so small although the substantial transfer to BF_4^- may be concerned.

All the above problems should be concerned with the uncertainty of the definition of charge transfer. Especially in metal-molecular or metal-inorganic solid interfaces, the detailed features of interface charge transfer cannot be described by the Voronoi decomposition, where only the integrated or averaged quantities are evaluated using only mathematical sectioning of space. More detailed analysis of the charge redistribution should be performed as cases of metal/oxide interfaces.[27,28,56]

Figure 10 shows the detailed analysis of the charge redistribution in forming the interface. From the charge-density grid data of the optimized adsorption system, we subtracted a simple superposition of each charge-density data of the EMIM-BF_4 system and of the Li slab obtained with the same atomic positions in the same supercell as the optimized adsorption system. In order to examine the nature of the charge transfer toward $EMIM^+$, we also obtained the charge-distribution change from $EMIM^+$ to $EMIM^•$ using the frozen configuration of the isolated $EMIM^+$ molecule as shown in Fig. 10(a). Figures 10(b) and 10(c) indicate that the charge-distribution changes associated with EMIM are quite different for Li and Au surfaces. For the on-top adsorption on a Li (100) surface [Fig. 10(b)], the charge increase at EMIM has some similarity to the features of $EMIM^•$ in Fig. 10(a) although the magnitude of the increase at EMIM is quite small and there are also some increases at the interface region indicated by an arrow. It seems that this feature is caused by the hybridized states between the LUMO-like states and metallic Li states as the DOS tail at the Fermi level, as can be seen in Fig. 3. Thus the charge transfer to $EMIM^+$ in the Li case contains intermediate or ongoing change to partial radical formation. For the on-top adsorption on a Au (100) surface [Fig. 10(c)], however, only the interface charge in-

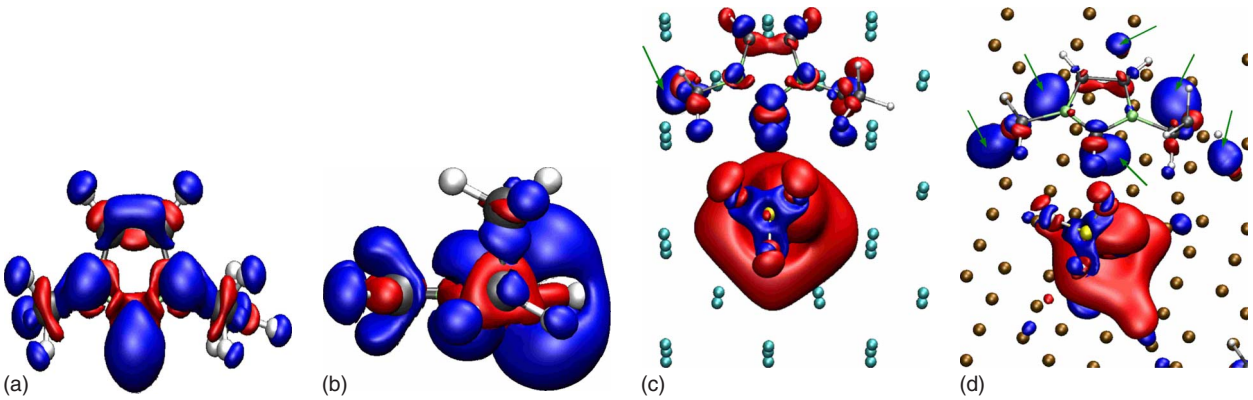

FIG. 10. (Color online) Charge-density redistribution (a) for $EMIM^{\bullet}$ against $EMIM^{+}$, (b) for EMIM-BF_4 side-on on-top adsorption on Li(100) against the superposition of EMIM-BF_4 and Li(100), and (c) for EMIM-BF_4 side-on on-top adsorption on Au(100) against the superposition of EMIM-BF_4 and Au(100). For the charge differences, isodensity surface is plotted for $0.01e/\text{Å}^3$ for (a) $EMIM^{\bullet}$, and $0.005e/\text{Å}^3$ for the adsorption systems (b) and (c), where red and blue mean charge depletion and charge accumulation, respectively. Green arrows in (b) and (c) indicate a charge accumulation on the surface under the EMIM ion.

creases are remarkable as indicated by arrows, and there is no specific electronic behavior to reduce $EMIM^{+}$. This indicates that the evaluated charge transfer by the Voronoi scheme is only the interface electron accumulation under the molecule and not the true transfer to $EMIM^{+}$ in the chemical viewpoint. This is the reason why the shift of the EMIM-DOS is negligible in spite of the substantial transfer in the Voronoi decomposition for the Au case.

It should be also noted that DFT fails to describe dispersive interactions such as Van der Waals within, for example, ionic liquid crystals.[57] This does not affect much results for EMIM-BF_4@Li systems since chemisorbed species are not highly influenced by such effect but can be of importance within some less interacting physisorbed systems such as organic molecules on gold, as examined in Ref. 58.

IV. CONCLUSIONS

The calculated results on each $EMIM^{+}$ and BF_4^{-} molecule, EMIM-BF_4 pair, and Li bulk and surfaces are in good agreement with other theoretical and experimental results. The EMIM-BF_4 adsorption on the Li surfaces has been examined to understand the primary interactions at ionic liquids/Li interfaces. So far, excluding end-on adsorptions, we have observed similar behavior regardless of the configurations or surfaces: one or two surface Li atoms are greatly attracted to BF_4, leading to local charge-density depletion in the surface and electron transfer toward $EMIM^{+}$. This process can be modeled by the following equation:

$$x\text{Li}_0 + \text{EMIM}^{+}\text{-BF}_4^{-} \rightarrow \text{EMIM}^{*} + (\text{Li}_x\text{-BF}_4)^{*}, \quad (5)$$

where * stands for adsorbed species, EMIM ion in $EMIM^{*}$ is intermediate between $EMIM^{+}$ and $EMIM^{\bullet}$, and $(Li_x\text{-}BF_4)^{*}$ is the precursor of a $Li^{+}\text{-}BF_4^{-}$ molecule. The energy gain of this process ranges from 0.81 to 1.45 eV.

It should be noted that there occurs no complete redox reactions generating Li^{+} ions or EMIM radicals at least within the present examination. However, we have observed such tendencies of easy ionization of Li and partial reduction in $EMIM^{+}$, which may be observed clearly for future computations using more realistic models of RTILs or charged electrode similar to the recent experimental models on metal-RTILs interfaces, as reviewed by Aliaga *et al.*[59] Moreover, on the experiments of the EMIM-BF_4/Li system, LiF layers are formed as solid electrolyte interphase (SEI),[60] which should be also examined in the future. In any case, it should be emphasized that the present results of the EMIM-BF_4 adsorption on Li surfaces indeed represent the electrochemical aspects of the EMIM-BF_4/Li system as compared with the EMIM-BF_4/Au system, for which no tendency of Au ionization or EMIM reduction has been observed.

ACKNOWLEDGMENTS

The present study was supported by Grant-in-Aid for Scientific Research (KAKENHI) on Priority Areas, "Science of Ionic Liquids," MEXT, Japan. The authors acknowledge the Tsukuba Advanced Computing Center and Tokyo University for computer time allocation.

*hubert.valencia@aist.go.jp

[1] F. Endres and S. Z. El Abedin, Phys. Chem. Chem. Phys. **8**, 2101 (2006).

[2] H. Sakaebe, H. Matsumoto, and K. Tatsumi, Electrochim. Acta **53**, 1048 (2007).

[3] B. Garcia, S. Lavallée, G. Perron, C. Michot, and M. Armant, Electrochim. Acta **49**, 4583 (2004).

[4] H. Sakaebe and H. Matsumoto, Electrochem. Commun. **5**, 594 (2003).

[5] H. Sakaebe, H. Matsumoto, and K. Tatsumi, J. Power Sources

146, 693 (2005).
[6] H. Matsumoto, H. Sakaebe, and K. Tatsumi, J. Power Sources **146**, 45 (2005).
[7] H. Matsumoto, H. Sakaebe, K. Tatsumi, M. Kikuta, E. Ishiko, and M. Kono, J. Power Sources **160**, 1308 (2006).
[8] C. P. Grey and N. Dupré, Chem. Rev. (Washington, D.C.) **104**, 4493 (2004).
[9] I. W. Seong, C. H. Hong, B. K. Kim, and W. Y. Yoon, J. Power Sources **178**, 769 (2008).
[10] A. Bagno, F. D'Amico, and G. Saielli, J. Mol. Liq. **131-132**, 17 (2007).
[11] M. G. del Pópolo, J. Kohanhoff, R. M. Lynden-Bell, and C. Pinilla, Acc. Chem. Res. **40**, 1156 (2007).
[12] M. G. del Pópolo, J. Kohanhoff, R. M. Lynden-Bell, and C. Pinilla, J. Phys. Chem. B **109**, 5895 (2005).
[13] Z. Meng, A. Dölle, and W. R. Carper, J. Mol. Struct.: THEOCHEM **585**, 119 (2002).
[14] Z. Liu, S. Huang, and W. Wang, J. Phys. Chem. B **108**, 12978 (2004).
[15] J. de Andrade, E. S. Böes, and H. Stassen, J. Phys. Chem. B **106**, 13344 (2002).
[16] S. A. Katsyuba, P. J. Dyson, E. E. Vandyukova, A. V. Chernova, and A. Vidiš, Helv. Chim. Acta **87**, 2556 (2004).
[17] R. Lü, Z. Cao, and G. Shen, J. Nat. Gas Chem. **16**, 428 (2007).
[18] S. Tsuzuki, H. Tokuda, K. Hayamizu, and M. Watanabe, J. Phys. Chem. B **109**, 16474 (2005).
[19] P. A. Hunt, I. R. Gould, and B. Krichner, Aust. J. Chem. **60**, 9 (2007).
[20] J. C. Soetens, C. Millot, and B. Maigret, J. Phys. Chem. A **102**, 1055 (1998).
[21] N. E. Heimer, R. E. del Sesto, and W. R. Carper, Magn. Reson. Chem. **42**, 71 (2004).
[22] J. S. Wilkes and M. J. Zaworotko, J. Chem. Soc., Chem. Commun. **13**, 965 (1992).
[23] K. Hayamizu, Y. Aihara, H. Nakagawa, T. Nukuda, and W. S. Price, J. Phys. Chem. B **108**, 19527 (2004).
[24] M. Otani and O. Sugino, Phys. Rev. B **73**, 115407 (2006).
[25] M. Otani, I. Hamada, O. Sugino, Y. Morikawa, Y. Okamoto, and T. Ikeshoji, J. Phys. Soc. Jpn. **77**, 024802 (2008).
[26] M. W. Finnis, J. Phys.: Condens. Matter **8**, 5811 (1996).
[27] S. Tanaka, R. Yang, and M. Kohyama, Philos. Mag. **86**, 5123 (2006).
[28] S. Shi, S. Tanaka, and M. Kohyama, J. Am. Ceram. Soc. **90**, 2429 (2007).
[29] G. Kresse and J. Hafner, Phys. Rev. B **47**, 558 (1993).
[30] G. Kresse and J. Furthmüller, Phys. Rev. B **54**, 11169 (1996).
[31] J. P. Perdew and Y. Wang, Phys. Rev. B **45**, 13244 (1992).
[32] P. E. Blöchl, Phys. Rev. B **50**, 17953 (1994).
[33] G. Kresse and D. Joubert, Phys. Rev. B **59**, 1758 (1999).
[34] J. P. Perdew, K. Burke, and M. Ernzerhof, Phys. Rev. Lett. **77**, 3865 (1996).
[35] H. J. Monkhorst and J. D. Pack, Phys. Rev. B **13**, 5188 (1976).
[36] J. D. Pack and H. J. Monkhorst, Phys. Rev. B **16**, 1748 (1977).
[37] G. Makov and M. C. Payne, Phys. Rev. B **51**, 4014 (1995).
[38] J. Neugebauer and M. Scheffler, Phys. Rev. B **46**, 16067 (1992).
[39] G. F. Voronoi and Z. Reine, J. Reine Angew. Math. **134**, 198 (1908).
[40] N. N. Medvedev, J. Comput. Phys. **67**, 223 (1986).
[41] A. D. Becke, J. Chem. Phys. **88**, 2547 (1988).
[42] J. P. Day and A. L. Ruoff, Phys. Status Solidi A **25**, 205 (1974).
[43] M. S. Anderson and C. A. Swenson, Phys. Rev. B **31**, 668 (1985).
[44] K. Doll, N. M. Harrison, and V. R. Saunders, J. Phys.: Condens. Matter **11**, 5007 (1999).
[45] K. Kokko, P. T. Salo, R. Laihia, and K. Mansikka, Surf. Sci. **348**, 168 (1996).
[46] A. Elaiwi, P. B. Hitchcock, K. R. Seddon, N. Srinivasan, Y. M. Tan, T. Welton, and J. A. Zora, J. Chem. Soc. Dalton Trans. **1995**, 3467.
[47] J. P. Foster and F. Weinhold, J. Am. Chem. Soc. **102**, 7211 (1980).
[48] A. E. Reed and L. A. Curtiss, Chem. Rev. (Washington, D.C.) **88**, 899 (1988).
[49] R. S. Mulliken, J. Chem. Phys. **23**, 1833 (1955).
[50] G. Henkelman, A. Arnaldsson, and H. Jónsson, Comput. Mater. Sci. **36**, 354 (2006).
[51] C. I. Bayly, P. Cieplak, W. D. Cornell, and P. A. Kollman, J. Phys. Chem. **97**, 10269 (1993).
[52] B. H. Besler, K. M. Merz, Jr., and P. A. Kollman, J. Comput. Chem. **11**, 431 (1990).
[53] U. C. Singh and P. A. Kollman, J. Comput. Chem. **5**, 129 (1984).
[54] J. S. Francisco and I. H. Williams, J. Phys. Chem. **94**, 8522 (1990).
[55] S. Shi, S. Tanaka, and M. Kohyama, Mater. Trans. **47**, 2696 (2006).
[56] R. Benedek, M. Minkoff, and L. H. Yang, Phys. Rev. B **54**, 7697 (1996).
[57] M. G. del Pópolo, C. Pinilla, and P. Ballone, J. Chem. Phys. **126**, 144705 (2007).
[58] K. Lee, J. Yu, and Y. Morikawa, Phys. Rev. B **75**, 045402 (2007).
[59] C. Aligara, C. S. Santos, and S. Baldelli, Phys. Chem. Chem. Phys. **9**, 3683 (2007).
[60] E. Peled, J. Electrochem. Soc. **126**, 2047 (1979).